




Article

The Role of Undecenoic Acid on the Preparation of Decorated MCM-41/Polyethylene Hybrids by In Situ Polymerization: Catalytic Aspects and Properties of the Resultant Materials

María L. Cerrada ^{1,*} , Artur Bento ², Ernesto Pérez ¹, João P. Lourenço ^{2,3}  and M. Rosário Ribeiro ^{2,*} 

¹ Instituto de Ciencia y Tecnología de Polimeros (ICTP-CSIC), Juan de la Cierva 3, 28006 Madrid, Spain; ernestop@ictp.csic.es

² Centro de Química Estrutural, Institute of Molecular Sciences, Departamento de Engenharia Química, Instituto Superior Técnico, Universidade de Lisboa, Av. Rovisco Pais, 1049-001 Lisboa, Portugal; artbento@itqb.unl.pt (A.B.); jlouren@ualg.pt (J.P.L.)

³ Faculdade de Ciências e Tecnologia, Universidade do Algarve, Campus de Gambelas, 8005-139 Faro, Portugal

* Correspondence: mlcerrada@ictp.csic.es (M.L.C.); rosario@tecnico.ulisboa.pt (M.R.R.)

Abstract: Functionalized polyethylene-based nanocomposites were prepared by in situ polymerization of ethylene with modified or neat MCM-41 nanoparticles (NMCM-41). Two different synthetic approaches were investigated to improve the compatibility between the hydrophobic HDPE matrix and the hydrophilic NMCM-41: (i) incorporation of UA into the polymeric matrix by copolymerization with ethylene, promoted by the zirconocene catalyst under homogeneous conditions, in the presence of pristine NMCM-41; (ii) use of undecenoic acid (UA) as an interfacial agent to obtain decorated NMCM-41 to be used as nanofiller for the in situ ethylene polymerization, catalyzed by $\text{Cp}_2\text{ZrCl}_2/\text{MAO}$ under supported conditions. The strong polar character of the carboxylic group is expected to either increase the hydrophilicity of the HDPE chains (strategy i) or interact with the NMCM-41 surface and provide an additional link to the polymeric chains via copolymerization of the vinyl group under supported conditions (strategy ii). Although metallocene catalysts have been shown to copolymerize olefins with functional monomers, the presence of oxygen-containing compounds in the reaction media strongly affects the polymerization activity as a result of the interaction of functional groups with the electrophilic active center of the catalyst. Thus, UA was pre-contacted with tri(isobutyl)aluminum (TIBA) prior to its use in the polymerization to reduce the deactivating character of the carboxylic acid groups towards the zirconocene catalyst. The influence of the UA presence on the polymerization behavior of the protection step is discussed, and the polymerization activities observed for the different approaches are compared. In addition, the thermal behavior and structural details of the resulting materials have been characterized. The impact of using neat or functionalized NMCM-41 on the final dispersion within the polymeric matrix is also analyzed, which is correlated with the mechanical performance exhibited by these HDPE-UA-NMCM-41 nanocomposites.

Keywords: polyethylene; undecenoic acid; MCM-41; nanocomposites; dispersion; crystallinity; stiffness



Citation: Cerrada, M.L.; Bento, A.; Pérez, E.; Lourenço, J.P.; Ribeiro, M.R. The Role of Undecenoic Acid on the Preparation of Decorated MCM-41/Polyethylene Hybrids by In Situ Polymerization: Catalytic Aspects and Properties of the Resultant Materials. *Catalysts* **2023**, *13*, 1182. <https://doi.org/10.3390/catal13081182>

Academic Editors: Piotr Bartczak, Jaroslaw Polanski and Tomasz Siudyla

Received: 29 June 2023

Revised: 20 July 2023

Accepted: 31 July 2023

Published: 2 August 2023



Copyright: © 2023 by the authors. Licensee MDPI, Basel, Switzerland. This article is an open access article distributed under the terms and conditions of the Creative Commons Attribution (CC BY) license (<https://creativecommons.org/licenses/by/4.0/>).

1. Introduction

In recent years, the development of high-performance polyolefin materials that combine their desirable properties with enhanced functionality and performance has received considerable attention. In particular, functional polyolefins and polyolefin nanocomposites have shown remarkable potential to address current challenges and drive innovation for these materials while opening up new opportunities in a wide range of industries. Indeed, the introduction of functional groups into polyolefin chains can result in materials with improved dyeability and adhesion properties, as well as better compatibility with non-olefinic polymers. Several examples in the literature describe the preparation of

functional polyolefins either by direct copolymerization of functional comonomers or by post-polymerization chemical functionalization [1–7].

Metallocene/MAO catalytic systems have been used for the copolymerization of ethylene with olefins containing hydroxyl or carboxyl groups. However, a large loss of catalytic activity is observed, compared to the values found in homopolymerization, due to the formation of stable complexes or salts between the functional monomer and the electrophilic active center of the catalyst. The use of aluminum alkyls, which react with the functional group of the comonomer to form O-Al bonds, can significantly reduce the negative effect of the comonomer on the catalyst [8–11].

Another way to improve the performance of polyolefins is to take advantage of nanotechnology to enhance their thermal, mechanical, and barrier properties [12–16]. By dispersing nano-sized fillers (layered silicates, carbon nanotubes, etc.) into the polymeric matrix, the final performance can be significantly improved beyond the limits of conventional polyolefins. Preparation routes that can enhance filler dispersion and interfacial adhesion are highly desirable, especially in the case of non-polar hydrophobic polymeric matrices, such as polyolefins, and polar hydrophilic fillers. In situ polymerization has been considered a very promising route for the preparation of polyolefin-based nanocomposites [17–24]. This approach has been reported to favor filler distribution and, importantly, can provide additional degrees of freedom to either use suitable decorated filler nanoparticles or modify the polymeric matrix by copolymerization with a comonomer containing appropriate functional groups, thus also promoting interfacial adhesion. A variety of inorganic materials are currently available as fillers [25,26].

In recent years, ordered mesoporous silicas of the M41S class have attracted great attention in numerous applications. The nanometric pores, together with the high porosity and surface area, make these silicas suitable supports for single-site catalysts [14,27,28], while the polymerization within the nanometric pores of the support increases the interfacial contact between the two dissimilar phases (hydrophilic silica and growing hydrophobic macrochains), contributing to improving the mechanical response of the final composite materials. Previous works have shown that the use of metallocene catalysts supported on MCM-41 gave rise to catalytic systems with interesting properties in terms of activity and polymer properties as a result of the confinement effects that can arise from the polymerization inside the porous structure, thus allowing the synthesis of hybrid organic-inorganic materials by in situ polymerization of ethylene over a wide range of nanofiller concentrations [21,29].

On the other hand, the surface reactivity of mesoporous silica facilitates its chemical modification and can increase the phase compatibility through better interfacial adhesion between the decorated MCM-41 particles used as filler and the polymeric matrix. The use of various interfacial agents (including different organosilanes with reactive end groups) for surface modification of mesoporous silica and further use in the preparation of polyethylene-based nanocomposites has been reported in the literature [15,19,30,31]. More specifically, the use of micro-sized MCM-41 particles and undecenoic acid (UA) for the preparation of MCM-41/HDPE hybrid materials by in situ polymerization has been explored in an attempt to enhance the final properties by improving the interfacial interactions between both components [32]. These hybrid materials containing MCM-41 particles showed better final mechanical performance along with an interesting gas permeation behavior without varying the processing temperature [20]. However, they underwent some oxidative degradation during processing. It was also shown that the incorporation of low amounts of UA as a comonomer is a suitable way to control the degradation of polyethylene.

In the present work, decorated polyethylene-based nanocomposites were prepared by in situ homo- or copolymerization of ethylene in the presence of MCM-41 nanoparticles (NMCM-41). The use of these nanoparticles can significantly affect both the polymerization activity of the supported single-site catalyst (as a result of differences in internal diffusion resistance and accessibility of active sites) and the performance of the resulting

nanocomposites by creating a significant fraction of interfacial polymer with properties different from those of the bulk polymer, even at low loading, compared to that existing when microparticles are added. In order to create favorable interfacial interactions between the two components, the use of NMCM-41 and UA (either as a comonomer unit or as an interfacial agent) has been combined, and different *in situ* polymerization methodologies have been implemented, using $\text{Cp}_2\text{ZrCl}_2/\text{MAO}$ as a catalytic system. These approaches basically consist of: (i) the introduction of polar groups into the polyethylene matrix by copolymerization of ethylene with UA in the presence of pristine NMCM-41; (ii) the initial surface functionalization of NMCM-41 with UA for their further use as filler and catalyst support for the zirconocene/MAO complex. In order to reduce the deactivating character of the carboxylic acid groups towards the zirconocene catalyst, UA was pre-contacted with tri(isobutyl)aluminum (TIBA) prior to incorporation into the polymerization reaction. Therefore, the influence of the presence of UA (as an interfacial modifier of NMCM-41 or as a functional comonomer) and its protection with TIBA on the polymerization behavior is discussed, and the reaction activities observed for the different approaches are compared. Furthermore, the thermal behavior as well as the structural and morphological details of the resulting materials are discussed and correlated with the mechanical performance exhibited by these HDPE-UA-NMCM-41 nanocomposites.

2. Results and Discussion

2.1. Characterization of NMCM-41

The synthesis of NMCM-41 was performed using the co-condensation method. The morphology of the resultant nanoparticles is highlighted in Figure 1. The scanning electron microscopy (SEM) image (Figure 1a) shows the presence of well-defined spherical nanoparticles with diameters of approximately 70 nm, while the transmission electron microscopy (TEM) image (Figure 1b) indicates the formation of a disordered pore structure.

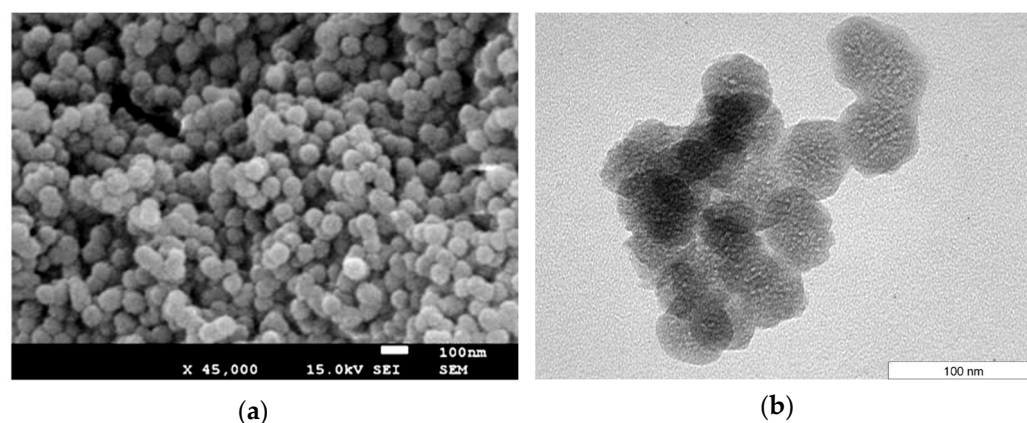


Figure 1. NMCM-41: (a) SEM images; (b) TEM micrographs.

The nitrogen sorption isotherm for MCM-41 nanoparticles is shown in Figure S1. This N_2 adsorption curve is slightly different from the typical isotherm exhibited by MCM-41 microparticles (type IV). In fact, the step corresponding to the capillary condensation of nitrogen inside the mesopores is not clearly evident. This feature indicates that the mesopores present in NMCM-41 have a less ordered arrangement than those present in the MCM-41 microparticles, as confirmed by the corresponding X-ray profiles represented in Figure S2 and the TEM image in Figure 1b. In addition, greater N_2 uptake occurs at high relative pressures (P/P_0 close to 1), which is expected for a material containing nanoparticles that give rise to a significant interparticle volume. These N_2 sorption measurements indicate a BET surface area of $726 \text{ m}^2/\text{g}$, a total porous volume (at $p/p_0 = 0.98$) of $1.68 \text{ cm}^3/\text{g}$, and a porous volume corresponding to the particle mesopores of $0.35 \text{ cm}^3/\text{g}$. Accordingly, this

material has a lower surface area and a smaller pore volume compared to those of the corresponding MCM-41 microparticles reported previously [19].

The FTIR spectra for the neat NMCM-41 material and the UA-functionalized sample are shown in Figure S3. The spectrum of the neat material shows the typical features of mesoporous silicas, with bands characteristic of OH stretching for isolated and interacting silanol groups at about 3740 and 3500 cm^{-1} [20,33,34], respectively, and bands at 2100–1600 cm^{-1} , corresponding to combination and overtone bands of Si-O network bonds.

After modification with the UA/TIBA interfacial agent, the band at 3740 cm^{-1} vanishes and new bands appear in the spectrum at 2927, 2856, and 3078 cm^{-1} , corresponding to the stretching modes of C-H in CH_2 groups and in double bonds [20,33–35]. Moreover, bands centered at 1581 and 1468 cm^{-1} , characteristic of carboxylate-type species in different coordination modes [20,35,36], are also visible. These results indicate that carboxyl groups with anionic character have been developed after UA/TIBA/NMCM-41 interaction, suggesting an effective interaction between the UA/TIBA and the silanol surface groups of the MCM-41 nanoparticles. Previous data from N_2 adsorption isotherms, thermogravimetric analysis, and FTIR spectroscopy also indicated that UA/TIBA species are retained in MCM-41 microparticles, effectively changing the MCM-41 surface and probably making the surface more hydrophobic [20].

2.2. Preparation of PE-UA-NMCM-41 Nanocomposites

Polymerization Behavior

Nanocomposites consisting of polyethylene and mesostructured silica particles with controlled morphology and nanometric size have been synthesized by in-situ polymerization using MAO-activated Cp_2ZrCl_2 as catalyst, either under homogeneous or supported conditions.

Two approaches were explored in order to create favorable interactions at the interface of both components: (a) the functionalization of the polyethylene matrix through copolymerization with UA, which is a polar comonomer (method A); and (b) the modification of the surface of NMCM-41 with UA, now used as an interfacial agent (method B). As commented in the Introduction, polar monomers are known to have a very detrimental effect on the catalytic activity of metallocene catalysts since they can coordinate with the electrophilic active centers, forming stable complexes and preventing the subsequent η^2 -alkene coordination [37]. The choice of polar monomers with several methylene spacers between the double bond and the polar functional group, as well as the protection of the functional group prior to polymerization reactions, are approaches that have been used to reduce this problem [38]. Trimethylaluminum (TEA), either alone or as a component of commercial methylaluminoxane [10,11,39,40], has been found to reduce the significant loss in activity, although complete protection cannot be achieved.

As aforementioned, UA, which is a long-chain α -olefin with a carboxylic group and, then, a strong polar character, was selected in this work as a comonomer and interfacial agent. UA was reacted with TIBA prior to its introduction into the polymerization medium. The high steric effect of bulky alkylaluminum may boost polar group protection. It should also be noted that previous studies on ethylene and UA copolymers showed a reduction in crystallinity and crystallite size with increasing UA content, which can negatively affect the mechanical performance of the final nanocomposite materials [11,32]. Therefore, the UA content in the final nanocomposites is attempted to be maintained low enough (less than 2 mol%) to balance the positive effect at the organic/inorganic interface and the negative effect related to the disruption of the regularity in the macromolecular chains due to the presence of UA.

Briefly, the following approaches were explored: Method A consists of the copolymerization of ethylene with UA, catalyzed by the homogeneous zirconocene complex, in the presence of neat NMCM-41. The polymerization of ethylene is conducted in method B in the presence of NMCM-41 decorated with UA, acting as catalyst support and filler.

The data presented in Table 1 show a summary of the polymerization conditions and the activity for the two methodologies used. The polymerization times were varied to attain an NMCM-41 content in the final nanocomposite of about 10%. For comparison purposes, results obtained for the copolymerization of ethylene with UA (also pre-contacted with TIBA) promoted by the homogeneous catalyst in the absence of filler are also shown.

Table 1. Polymerization conditions, polymerization activities, and UA content (mol%) obtained for the nanocomposites prepared by the methods A and B and for the reference samples. In addition, the UA content in the final material (mol%) determined by ^1H NMR and the NMCM-41 amount incorporated and estimated by TGA are also provided.

Method and Sample Name	NMCM-41 Particles	Catalytic System	[UA] (10^{-5} M)	[Zr] (10^{-5} M)	Activity kgPE/molZr/h	UA mol%	NMCM-41 (% m/m)
REF1	-	Homog.	3.8	3.8	9100	0.7	0
REF2	-	Homog.	30.5	6.4	1200	n.d.	0
A1 ¹	Neat	Homog.	3.8	3.8	8560	n.d.	10
A2 ¹	Neat	Homog.	30.5	6.4	780	1.7	9
A3 ²	Neat	Homog.	30.5	6.4	1000	n.d.	10
B1 ¹	Decorated	Supported	3.8	3.8	620	1.3	11
B2 ²	Decorated	Supported	3.8	3.8	600	n.d.	9

$P_{\text{ethylene}} = 1.2$ bar, $T = 25$ °C, $\text{Al/Zr} = 1000$, mass of NMCM-41 = 100 mg. n.d.—not determined. The neat or modified NMCM-41 was dispersed in toluene prior to their introduction in the polymerization reactor: ¹ in an ultrasound bath for 15 min, and ² with an ultrasonication probe for 5 min.

Looking at the results obtained with method A, the introduction of the neat mesoporous silica filler in the reaction medium does not significantly influence the catalytic activity of the homogeneous metallocene/MAO catalytic system for the copolymerization of ethylene with UA. In fact, the activity values obtained for a given amount of catalyst and UA comonomer in the presence of NMCM-41 are similar to those obtained in their absence, as deduced when comparisons are stated between samples REF1 with A1 or REF2 with A2 or A3.

On the other hand, a significant decrease in the average polymerization activity is observed with the amount of UA in the reaction and the corresponding increase in the UA/Zr ratio. This trend is observed both for the copolymerization reactions performed in the presence of neat NMCM-41 (method A) or in its absence (reference tests). The above-mentioned deactivating character of the polar carboxylic groups towards the electrophilic active center of metallocene-type catalysts ($\text{Cp}_2\text{Zr}^+\text{CH}_3$) and an incomplete protection may explain the observed behavior. Although the high steric effect of bulky alkylaluminum could favor polar group protection, data show that complete protection could not be achieved, and free functional groups of deactivating nature may remain. The change in the protocol for the dispersion of NMCM-41 in toluene (sonication in a bath or using a probe) before their incorporation into the polymerization reactor does not have a very significant effect on the polymerization activity, although it might cause differences in the dispersion of NMCM-41 within the final nanocomposite materials.

An important decrease in activity is, however, noticed in the polymerization reactions performed with the catalyst supported on the surface of NMCM-41 previously modified with UA/TIBA (method B). This is a common behavior of many supported catalysts that are prepared by the impregnation procedure. Steric hindrance of the support, acting as an extremely bulky ligand, combined with inefficient active site generation or even deactivation of effectively generated active sites, are among the aspects that may influence the behavior observed here [18,41,42]. It should also be noted that the deactivation of the catalyst active sites can become extremely severe with this methodology. In fact, as NMCM-41 is modified with UA/TIBA prior to catalyst impregnation, the incomplete protection of the carboxylic groups by TIBA and the proximity of these polar groups to the catalyst active sites may enhance marked active site deactivation. On the other hand, the different

sonication procedures used for dispersing the decorated MCM-41 nanoparticles have no effect on polymerization activity, as already commented for method A.

Figure 2 compares representative kinetic profiles obtained in the ethylene/UA copolymerization tests performed under the above-mentioned methodologies. For the homogeneous $\text{Cp}_2\text{ZrCl}_2/\text{MAO}$ system, similar kinetic profiles are obtained for the samples prepared either in the presence or absence of NMCM-41, samples A1 and REF1, respectively. This means that MCM-41 nanoparticles do not interfere with the polymerization rate. Moreover, these kinetic profiles present the typical pattern observed for homogeneous metallocene catalysts in ethylene polymerization, where the activity peak is followed by a steady decline. Such behavior is usually attributed to bimolecular deactivation reactions between neighboring zirconocene sites [43]. On the other hand, the type of kinetic profile is dependent on the UA concentration. At low concentrations, the kinetic profile shows a high initial activity (see sample A1), which gradually decreases after reaching the maximum value, while the kinetic profile is characterized by a notably lower initial activity but is very stable over time at high concentrations (as depicted for specimens REF 2 and A2). Although polymerization activity in supported catalysts is significantly reduced relative to that observed under homogenous conditions, the immobilization of the catalyst inside the NMCM-41 channels may protect it against either bimolecular deactivation or comonomer deactivation during the polymerization, and, therefore, a very stable profile is also observed.

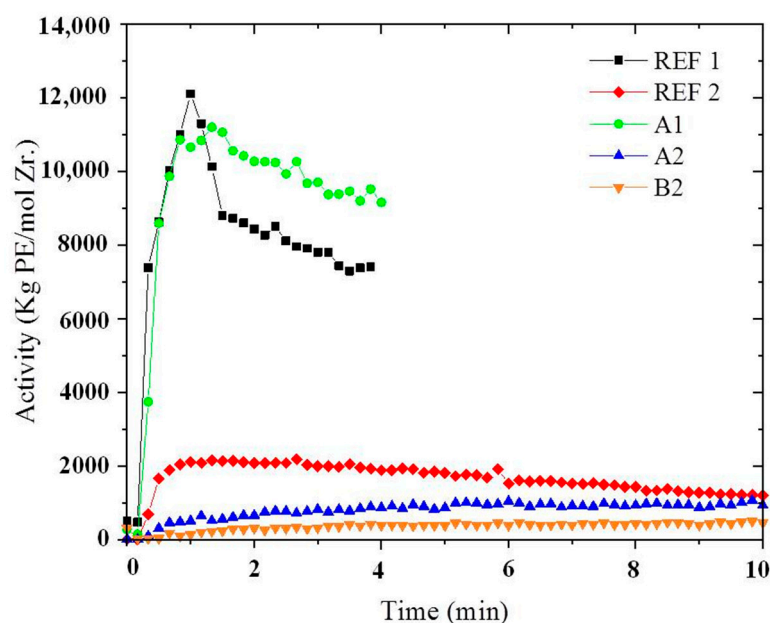


Figure 2. Kinetic profiles for ethylene copolymerization with the homogeneous catalyst in the absence or presence of pristine NMCM-41 (samples REF1, A1, and A2) and with the supported catalyst on modified NMCM-41 (B2).

Figure 3 shows the FTIR spectra of some nanocomposite specimens representative of the two methods used during the synthesis. The spectrum of sample REF1, which is the ethylene/UA copolymer, is also shown for comparison. The spectra of the nanocomposites clearly exhibit the characteristic bands of UA incorporation in acid and ester forms, at 1711 and 1746 cm^{-1} , respectively [10]. It should also be noted that the carboxylate species detected in the decorated MCM-41 particles are still present in the hybrids (bands at 1580 and 1626 cm^{-1}) even after extensive polymer washing. However, these bands are virtually absent in the neat copolymer used as a reference. Although the exact nature of the MCM-41/UA/TIBA/PE interactions is difficult to determine, these results seem to indicate a strong interaction between the mesoporous silica, the carboxylate species, and the polymeric matrix. Thus, an improvement in the adhesion between the organic polymer and

the inorganic filler is expected. It is also found that the intensity of the bands related to UA incorporation (acid and ester forms as well as carboxylate species) raises with increasing UA concentration in the reaction medium. Since the spectra of the nanocomposites are normalized with respect to the 720 cm^{-1} band, associated with the main polyethylene backbone, it follows that the higher the UA concentration in the feed, the greater the UA incorporation into the polyethylene macrochains.

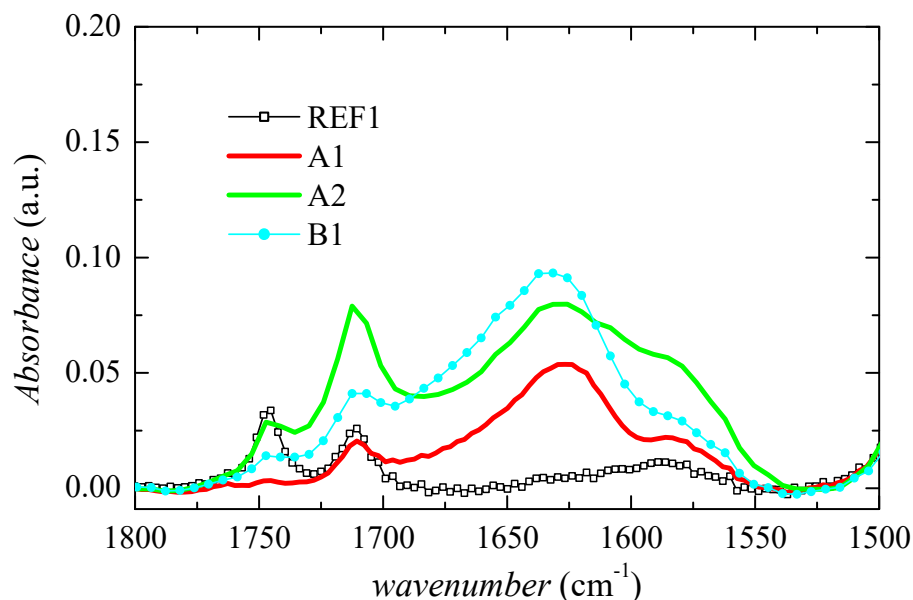


Figure 3. FTIR spectra of the REF1 (ethylene-UA copolymer) and the A1, A2, and B1 nanocomposites.

2.3. Study of PE-UA-NMCM-41 Nanocomposites

2.3.1. Thermal Stability

Once distinct nanocomposites have been achieved by the two methods aforementioned, analysis of their decomposition features is necessary. MCM-41 particles with micrometric sizes have sometimes been used as degradation catalysts [44]. In addition, films have been attained by compression molding, i.e., applying a temperature above the melting point of the polymeric matrix. Therefore, evaluating the thermal stability of the different materials is a very important aspect to learn. From these thermogravimetric experiments, the content of mesoporous silica can also be determined. This amount, estimated at a specific specimen, is quite independent of the atmosphere employed during the measurement. Thus, the values listed in Table 1 are the average data attained from the experiments performed under either inert or oxidative conditions.

Figure 4 displays the thermogravimetry curves obtained under the two experimental conditions used: inert and air atmospheres for the several nanocomposites. Their corresponding derivatives are represented in Figure S4 of the Supporting Information. The pristine ethylene-UA copolymer (sample REF1) has also been examined. A unique main stage of decomposition is noted in the temperature interval from 200 to 650 °C for REF1 and the several nanocomposites under inert conditions, as depicted in Figure 4a. The thermal degradation of pure polyethylene has been described as taking place under nitrogen atmospheres through a mechanism of random scission. This type of rupture leads to the fragmentation of initial polymeric macrochains into portions of different lengths. The process involves the random formation of free radicals along the polymeric backbone with subsequent scission of the molecule, resulting in the formation of one molecule with an unsaturated end and another with a terminal free radical. Thereafter, reactions of hydrogen chain transfer transform the radical segments into straight-chain dienes, alkenes, and alkanes [45].

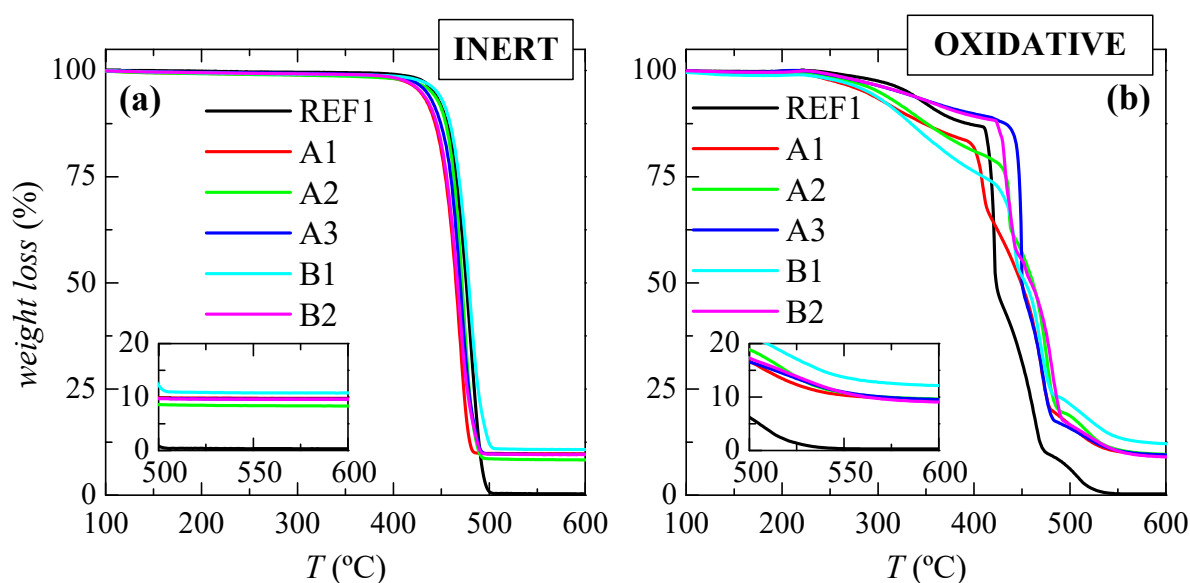


Figure 4. Thermogravimetry curves derived from experiments performed under (a) inert and (b) air atmospheres for the samples REF1 and the different nanocomposites synthesized by the two in-situ polymerization protocols.

The behavior is rather different when air is used as the environment. Then, four different degradation processes are clearly evident at the same temperature range. The early reaction of thermal oxidation in polyethylene consists of the development of alkyl radicals from its polymeric chains. The next stage implies the reaction of those alkyl radicals with oxygen to form hydroperoxides that can be decomposed into alkoxy radicals. Then, these alkoxy species abstract hydrogen from the macrochain, and other alkyl radicals are generated. Finally, various carbonyl species are produced.

The presence of a small amount of UA in the sample REF1 and in the nanocomposites does not affect much the thermal decomposition under inert atmosphere with respect to that exhibited by pure HDPE because the content in UA is maintained rather low, inferior to 2 mol% [20]. Under an oxidative environment, the REF1 specimen and the compounds with NMCM-41 show a small weight loss of about 1 wt.% (or less, depending on the UA amount) up to 200 °C associated with the dehydration of hydroxyl groups.

The mesoporous MCM-41 silica has been used as a degradation catalyst, as commented above. A significant displacement to lower temperatures of the main degradation process under inert conditions has been described with increasing MCM-41 content in nanocomposites based on ethylene and micrometric MCM-41 particles achieved by in-situ polymerization [29]. The effect of NMCM-41 on the degradation process is here less visible, both under inert or oxidizing atmospheres, contrary to what was described in those hybrids prepared with MCM-41 microparticles. The catalytic influence of the MCM-41 nanoparticles on the degradation of polyethylene chains is likely to be lower than that of the microparticles because of their smaller porous volume (0.35 cm³/g compared with 0.68 cm³/g exhibited by MCM-41 [19]), a fact that will reduce in an important extent the amount of polyethylene inside the nanometric channels.

The differences found between the distinct materials, mainly under oxidative conditions, can be associated with variations promoted by several factors that might affect the degradation in these systems: how the polymerization was carried out (under homogeneous or supported conditions); the amount of AU in the final nanocomposites; and the content of NMCM-41, among the most significant ones. To fully understand these differences, a more in-depth degradation study should have been carried out, which is outside the scope of this research.

2.3.2. Structural Characterization

Figure 5 shows the X-ray diffraction patterns at the wide-angle region, WAXD, for the neat ethylene-UA copolymer (sample REF1), the different nanocomposites, and the MCM-41 nanoparticles. All of them, except NMCM-41, exhibit at room temperature the orthorhombic polymorph that is the common crystalline lattice displayed by polyethylene and its derivatives. This cell is characterized by the presence of two main diffractions [46,47], the (110) and (200) reflections. The location of these two peaks is almost unchanged for the different specimens, independently of the absence or addition of NMCM-41 and of the way that these nanoparticles have been incorporated, i.e., simply as a filler during polymerization or playing the additional role of catalyst support. Accordingly, the size of the crystallite cell will remain nearly unaffected for these diffraction planes. Regarding the NMCM-41 material, its completely amorphous nature at this short range is clearly deduced from Figure 4.

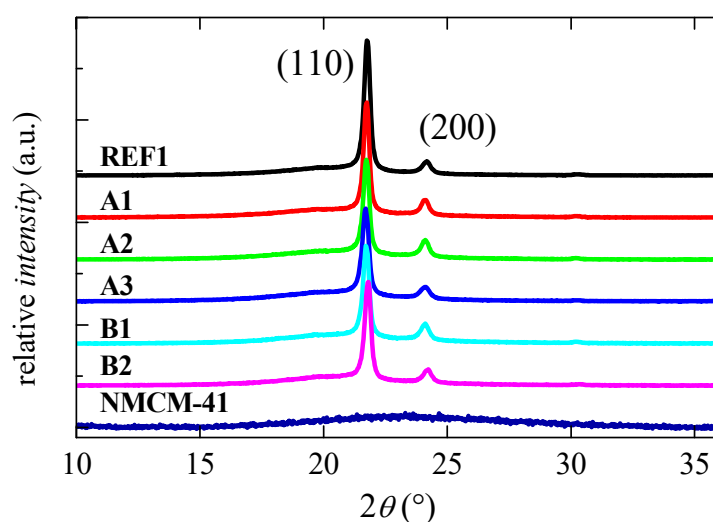


Figure 5. WAXD diffraction profiles at room temperature for the different samples analyzed: REF1, A1, A2, A3, B1, B2, and NMCM-41, from top to bottom.

Mesoporous MCM-41-type silicas are characterized as being amorphous in their bulk [48], showing ordered arrangements at longer spacing ranges, which indicate a hexagonal morphology between their channels, as deduced from Figure S2 of the Supporting Information. Similarly, NMCM-41 does not show any ordering at short range. Nevertheless, the small size of their spherical nanoparticles (see Figure 1) causes the void channels to lose their relative organized distribution in the long range. Thus, NMCM-41 shows a broad peak at low angles, pointing out its disorder (see Figure S2). The distinct nanocomposites show this broad reflection of NMCM-41 at a low angle (out of the scale of Figure 5), a fact that indicates that the nanoparticles have been incorporated during the synthetic stage. The intensity is much smaller since their content in the nanocomposites is lower than in pure NMCM-41.

2.3.3. Phase Transitions

Sample REF1 and the different nanocomposites are, as commented, semicrystalline. Thus, analysis of how the presence of MCM-41 nanoparticles affects the phase transitions of those orthorhombic crystallites turns out to be very interesting. Figure 6 shows the DSC curves attained during the initial heating run at 10 °C/min for all of those specimens processed as films after applying fast cooling. A unique melting endotherm is observed in the temperature interval represented. The maximum, which is considered the melting temperature of the specimens (T_m), is located at higher temperatures in the nanocomposites than in the REF1 sample, as listed in Table 2. This feature is an indication that the crystallite

size is greater in the nanocomposites. Thus, the presence of NMCM-41 boosts the growth of thicker crystals. A difference has also been observed when a comparison is established between the nanocomposites attained by the two different protocols. Those materials containing NMCM-41 and prepared under homogenous conditions during polymerization, i.e., ethylene-UA copolymers with neat silica nanoparticles (specimens A1, A2, and A3), show higher T_m than those where NMCM-41 was firstly modified with UA and, later, this decorated silica was used as catalyst support (samples B1 and B2). Pristine NMCM-41 seems to induce a greater influence on the development of larger crystallites in the copolymers, where their formation is more hindered by the presence of a small amount of UA counts. This favorable effect appears to be reduced by the functionalization of NMCM-41 with UA.

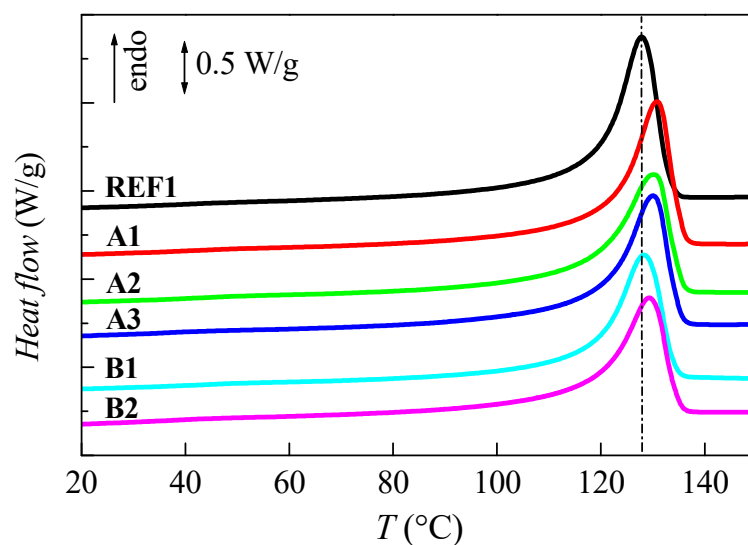


Figure 6. DSC curves during the first heating run, at 10 °C/min, for the REF1 sample and the A1, A2, A3, B1, and B2 nanocomposites, from top to bottom.

Table 2. NMCM-41 content in each material analyzed, estimated as a mean value from TGA experiments, together with melting and crystallization temperatures (T_m and T_c , respectively) and the normalized crystallinity degrees obtained from the first heating and cooling DSC experiments (f_c^{F1} and f_c^C , respectively).

Sample Name	NMCM-41 Content by TGA	T_m (°C)	f_c^{F1}	T_c (°C)	f_c^C
REF1	0	127.5	0.54	117.0	0.55
A1	10	131.0	0.54	118.0	0.52
A2	9	130.5	0.54	117.0	0.51
A3	10	130.0	0.53	116.0	0.50
B1	11	128.5	0.52	117.5	0.50
B2	9	129.5	0.51	118.0	0.49

This behavior is somehow different from that exhibited by the composites incorporating MCM-41 microparticles, where T_m was practically unaffected in all of the samples examined [32]. Another difference observed regarding the nanocomposites containing MCM-41 with micrometric size is that in these current nanocomposites with NMCM-41, only a single melting process takes place, while they showed the presence of a secondary endothermic event at around 80 °C. The existence of that process is indicative of the melting of crystals with significantly smaller sizes. Those thinner crystals were associated with the ones involving polymeric macrochains able to be organized three-dimensionally within the

nanometric MCM-41 channels. Obviously, these crystallites cannot grow larger because of the confinement exerted by the size of the MCM-41 pores. The lack of observation in these nanocomposites that contain NMCM-41 instead of MCM-41 is attributed not to the absence of polymeric chains within the nanometric spaces existing within these nanoparticles but to their much smaller amount. Now, the polymeric chains located inside the pores of NMCM-41 are comparatively much less, because of the small size and porous volume of these spherical nanoparticles, than those that could be confined within the channels with micrometric lengths. Accordingly, this secondary endothermic process is not noted because it cannot be detected or because it does not occur.

On the other hand, results reported in Table 2 also show that the degree of crystallinity does not follow the same trend as that noted in the T_m values. Thus, sample REF1 is able to develop a similar or higher number of crystallites than the nanocomposites, and its crystallinity is accordingly analogous or greater.

Figure 7 shows the calorimetric curves derived from the cooling DSC experiments. A clear crystallization process is noticed for all the different specimens. The location of the minimum of the crystallization, i.e., the crystallization temperature (T_c), for the different nanocomposites compared to that found in the sample REF1 (see values in Table 2) seems to be affected by several variables.

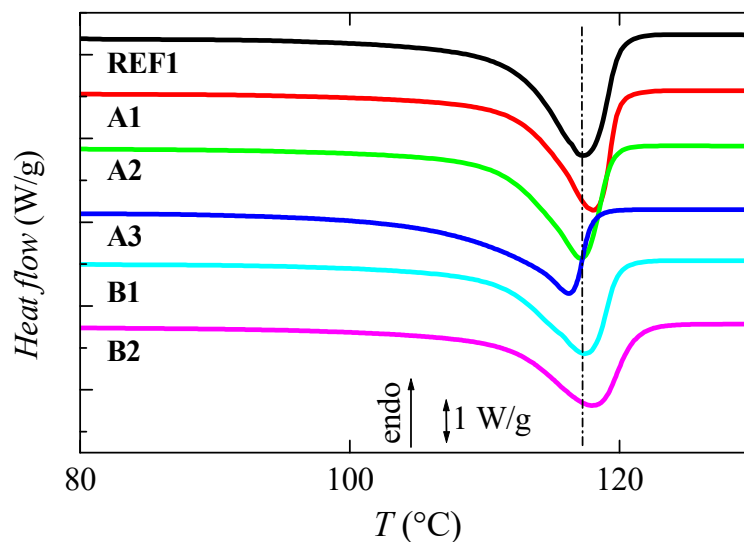


Figure 7. DSC curves during the cooling run, at 10 °C/min, for the REF1 sample and the A1, A2, A3, B1, and B2 nanocomposites, from top to bottom.

A nucleating effect of NMCM-41, shifting the T_c to a higher temperature, is noted as the A1 and REF1 samples are compared. Nevertheless, this behavior is not observed in the A2 and A3 nanocomposites, where constancy in the T_c position or its displacement to slightly lower temperatures is seen, respectively. This different trend, despite the fact that the content of NMCM-41 is rather similar in all of these materials, can be associated with an expected greater amount of UA within the macrochains of A2 and A3 specimens compared with that existing in the A1 sample since the UA concentration in the feed is much higher for those two A2 and A3 materials (see Table 1). It should be remembered that a larger content of UA incorporated into the polymeric chains interrupts the regularity of polyethylenic sequences and, then, their capacity for crystallization. Regarding the nanocomposites where NMCM-41 was first decorated with UA and further used as a catalyst carrier, the T_c appears for B1 at an analogous position to that in the REF1 sample, and it moves to a higher temperature in the B2 nanocomposite. Thus, the modified MCM-41 nanoparticles act as nucleants in the crystallization of polyethylene chains in the B2 material. It should be noted, however, that differences in T_c between the REF1 sample and the several nanocomposites are not very significant.

2.3.4. Morphological Details

The results explained above allow for the presumption that all of these nanocomposites, independently of incorporating neat or decorated NMCM-41, consist of polyethylene-based chains that primarily surround the NMCM-41 silica, with a small amount of them located within the nanochannels of these mesoporous NMCM-41. The content of polymeric macromolecules inside these confined spaces is too low due to the nanometric size of NMCM-41, whose diameter is about 70 nm (see Figure 1). The final properties are determined by the crystalline properties of the polymer matrix. However, they are also strongly influenced in nanocomposites by the morphological aspects derived from the distribution of the nanoparticles. Figure 8 shows the corresponding SEM images for the different nanocomposites, grouped according to the synthesis protocol that was used.

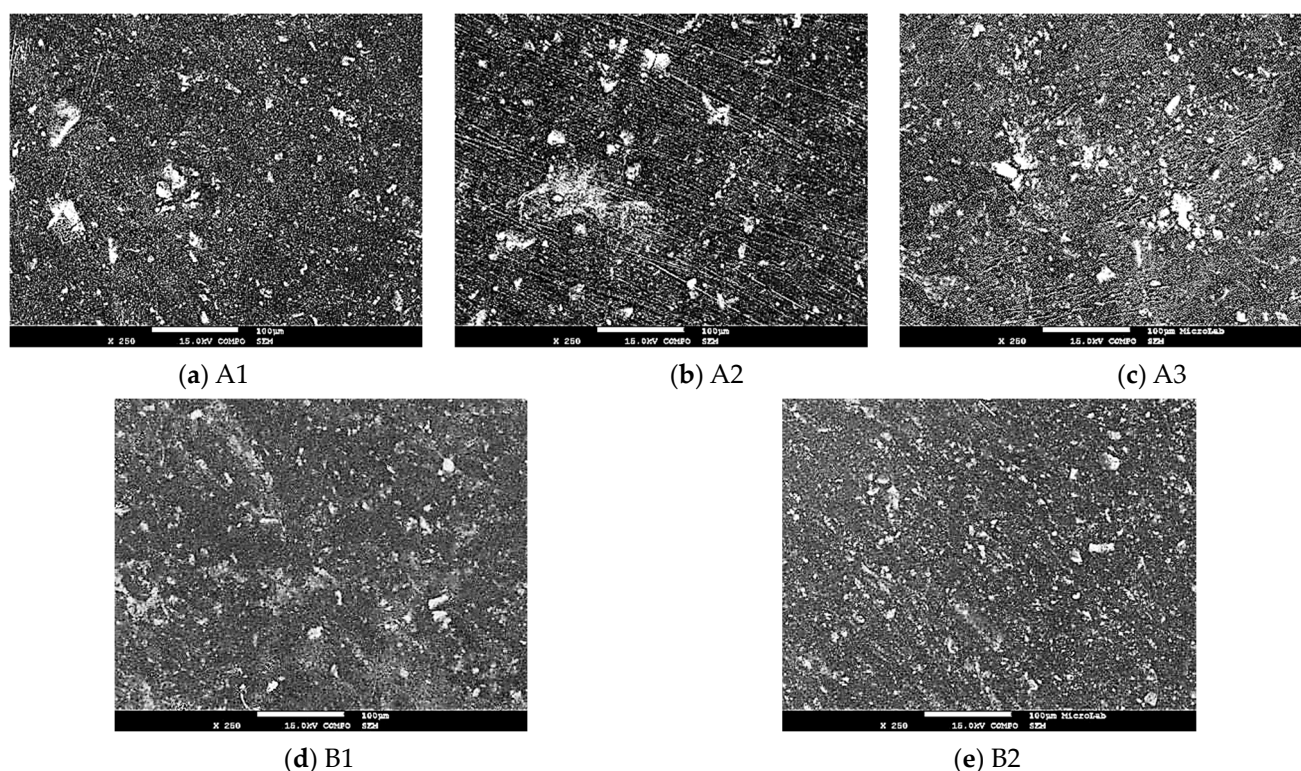


Figure 8. SEM microphotographs for the NMCM-41 nanocomposites using UA interfacial agent: UA group added into the polymeric matrix by copolymerization in the presence of neat NMCM-41 (pictures (a–c)); and, initial functionalization of NMCM-41 with UA before ethylene homopolymerization (pictures (d,e)).

This Figure depicts that the materials obtained using the method of modifying the polymeric matrix with UA (i.e., A1, A2, and A3) show the presence of some agglomerates of NMCM-41. The existence of these aggregates deteriorates the NMCM-41 dispersion, leading to its poor distribution. In spite of the small size of the spherical MCM-41 nanoparticles, the final morphology is not improved relative to that described previously in nanocomposites incorporating MCM-41 microparticles [32]. On the other hand, the formation of agglomerates takes place to a much smaller extent and size in the nanocomposites obtained by the modification of NMCM-41 with UA (these decorated nanoparticles having been later used also as catalyst support), i.e., in specimens B1 and B2. Therefore, a better dispersion of NMCM-41 is noticeable. No conclusion can be drawn regarding the protocol used (ultrasonic bath or probe) for the dispersion of nanoparticles before polymerization.

In order to attain further information about the morphological details of these nanocomposites, TEM micrographs have been carried out on samples A1 and B1, as shown in

Figure 9. Agglomerates in B1 appear to be more randomly distributed than in the material A1.

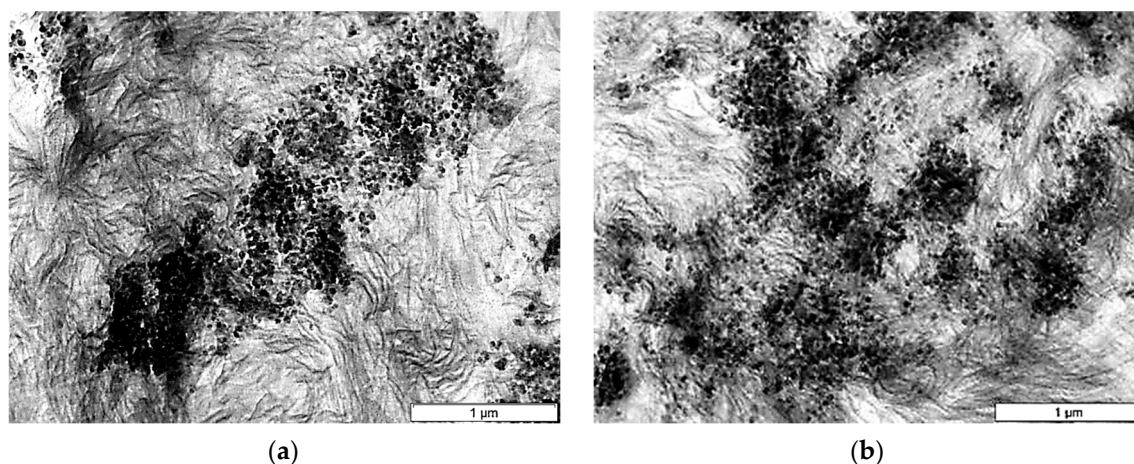


Figure 9. TEM microphotographs for two of the NMCM-41 nanocomposites: (a) A1 and (b) B1.

2.3.5. Viscoelastic Behavior

Once the crystalline characteristics and their phase transitions, together with the morphological information, are known, the relaxations existing in these materials as well as the dependence of storage moduli on temperature in a broad interval are studied.

Figure 10 shows the variation of the storage modulus (E') and the loss tangent ($\tan \delta$) for the sample REF1 and the different nanocomposites. A relatively small change is observed in the values of E' for all of the distinct specimens at low temperatures, which ranged from -150 to -25 °C, as displayed in the left plot of Figure 10. On the contrary, an important decrease of almost two orders of magnitude is observed from -25 to 120 °C. This is the common response to polyethylenic derivatives. Thus, incorporation of a content of around 10 wt.% in NMCM-41 does not alter this general behavior.

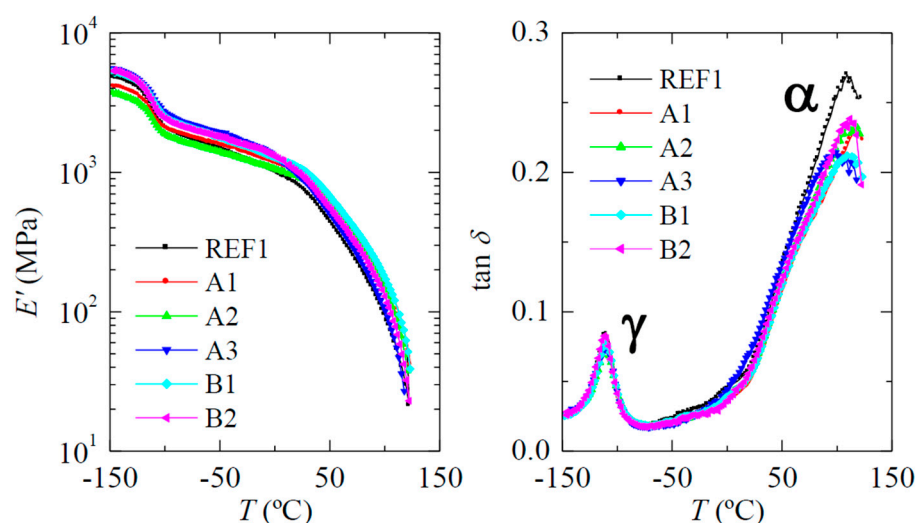


Figure 10. Dependence on temperature of storage modulus (left plot) and $\tan \delta$ (right plot) curves at a frequency of 3 Hz for the REF1 samples and the different nanocomposites.

A dependence of E' on the presence of nanoparticles of silica is, however, observed at 20 °C, as listed in Table 3. As expected, the sample REF1 shows the lowest value (825 MPa), while all of the nanocomposites exhibit higher storage moduli. In fact, the E' for the material A2, which is the one showing the smaller magnitude of the nanocomposites, is almost

15% higher than that for REF1. The increase in stiffness is related in the nanocomposites to several factors: crystallinity and crystal size of polymeric crystallites; incorporation of MCM-41 nanoparticles (their content is quite irrelevant since it is approximately the same for the different nanocomposites); their dispersion; and the absence of agglomerates. Taken into account all these parameters and looking at the data from Table 3, the nanocomposites that include the UA units in the polymeric macrochains adding neat NMCM-41 show an inferior stiffness at 20 °C than that found in the materials prepared using decorated NMCM-41 with UA. Two opposite features take place in these two sets of samples. The former shows a slightly higher degree of crystallinity and crystallite size (see Table 2), while the latest exhibits better morphological characteristics. Accordingly, it seems that the reinforcement effect of NMCM-41 is maximized in the nanocomposites with improved nanoparticle distribution, where their agglomeration is minimized, although the crystalline details of their matrix are slightly worse.

Table 3. Values of storage modulus E' at 20 °C together with the relaxation temperature for the two relaxation processes (on a $\tan \delta$ basis) at 3 Hz for the REF1 samples and the different nanocomposites. The content of NMCM-41 and the degree of crystallinity are also included.

Sample Name	NMCM-41 Content by TGA	f_c^{F1}	E' (MPa)	T (°C)	
				γ	α
REF1	0	0.54	825	−110.5	109.0
A1	10	0.54	1020	−110.0	117.5
A2	9	0.54	940	−110.0	113.5
A3	10	0.53	980	−110.0	104.0
B1	11	0.52	1110	−110.0	112.0
B2	9	0.51	1025	−111.5	111.5

The representation of $\tan \delta$ as a function of temperature (see the right plot in Figure 10) shows two viscoelastic relaxations taking place in this interval, which are labeled as γ and α in order of increasing temperatures. Some polyethylenic derivatives display another relaxation process, commonly identified as β , which is located between the γ and the α processes. It appears in low-density polyethylene, linear low-density polyethylene, and ethylene copolymers [49–51]. This β process is not clearly noticed in these specimens, although it could be masked and overlapped in the low-temperature region of the α mechanism. In addition, its intensity would be small because the UA content is quite low in the copolymers (inferior to 2 mol%) and, then, the degree of crystallinity in these samples is relatively high. Similar features were found in other HDPE samples [52].

The γ relaxation in polyethylene was initially associated with crankshaft movements of polymethylenic chains [53]. Nevertheless, there is no consensus concerning the details of the primary motional process [54]. Chains containing sequences of three or more methylenic units are required for this kind of movement. Figure 10 and the data in Table 3 show that the location of γ (based on the $\tan \delta$ maximum at 3 Hz) is not significantly affected by either the incorporation of NMCM-41 or its content. Thus, on the one hand, it appears at a quite analogous temperature in sample REF1 as in the nanocomposites, and, on the other hand, the amount of NMCM-41 is rather similar in all the materials analyzed. Motions associated with this relaxation occur in the amorphous regions. They seem, in principle, to be slightly hindered by the presence of NMCM-41, but its effect on the position is minimal.

The process that appears at higher temperatures, the α relaxation, has been associated with reorientational and vibrational movements within the crystallites [55,56]. The melting of the crystallites overlaps with this relaxation at the highest temperatures. As commented for the mobility within the amorphous regions, the motions occurring in the crystallites also become more hindered because of the presence of NMCM-41, and, therefore, the α process is displaced to higher temperatures and its intensity is now reduced.

3. Materials and Methods

3.1. Materials

All manipulations were performed under dry nitrogen using standard Schlenk techniques. Ethylene and nitrogen (Air Liquide) were purified through absorption columns containing molecular sieves 4A and 13X. methylaluminoxane (MAO, 7 wt.% in toluene solution, Akzo), Cp_2ZrCl_2 , tri(isobutyl)aluminum (TIBA), undecenoic acid (UA), tetraethyl orthosilicate (TEOS), diethanolamine (DEA), and cetyltrimethylammonium chloride (CTAC, 25% aq. Sol.) purchased from Aldrich, were used as received. Toluene (Petrogal) was distilled over sodium under a dry nitrogen atmosphere, using N-benzophenone as an indicator.

3.2. Preparation and Characterization of Neat and Modified NMCM-41

NMCM-41 was prepared following the work of [57]. In a typical synthesis, water (128 mL), CTAC solution (20.8 g), ethanol (96%, 18 g), and DEA (0.4 g) were mixed and stirred in a flask immersed in a water bath at 40 °C for 30 min. TEOS (14.6 mL) was then added to the mixture and stirred for 2 h. Then, the solution was cooled to room temperature, and the white powder was recovered by centrifugation, washed with water, and dried at 80 °C overnight. The template was partially removed with 96% ethanol by heating under reflux for 24 h. After drying, the product was calcined under a flux of air at 550 °C for 12 h.

The decoration of NMCM-41 using UA/TIBA as an interfacial agent was performed by the addition of a solution of UA reacted with TIBA (1:1 molar equivalent) to a slurry of MCM-41 (100 mg) in 4 mL of toluene for 16 h in a Schlenk flask under magnetic stirring.

The synthesized materials were analyzed by powder XRD in a Panalytical X'Pert Pro, using $\text{CuK}\alpha$ radiation filtered by Ni and an X'Celerator detector. SEM and TEM images were obtained on JEOL JSM-7001F equipment and on Hitachi H8100 equipment, respectively. Samples were deposited in a Cu/polymer grid sample holder.

FTIR spectra were recorded on a Thermo Nicolet Nexus instrument (64 scans with a resolution of 4 cm^{-1}). Self-supported wafers (~10 mg) were placed in an infrared quartz cell and then evacuated under primary vacuum (10^{-2} Torr) at 150 °C. The background spectrum, recorded under identical operating conditions, was automatically subtracted from each sample spectrum.

Nitrogen adsorption isotherms were measured at −196 °C in ASAP 2010 Micromeritics equipment. Samples were degassed at 300 °C for 3 h prior to the experiment. The specific surface area was estimated by the BET method, and the mesoporous volume was estimated by the *t*-plot method [58]. The total pore volume, which includes the interparticle volume and the particle mesoporous volume, was estimated from the N_2 adsorption isotherm at $p/p_0 = 0.98$.

3.3. Preparation of the Supported Catalyst on the Modified NMCM-41

In an inert schlenk, 1.1 mL of a 1.7×10^{-3} M solution of Cp_2ZrCl_2 in toluene was added to a suspension of 100 mg of the modified mesoporous silica support in 4 mL of toluene, previously sonicated. The suspension is placed under stirring for 5 h, protected from light.

3.4. Catalytic Tests

Polymerizations were performed in a dried and nitrogen-flushed bottle for pressure reactions (Wilmad LabGlass LG-3921) with magnetic stirring. Polymerizations were performed at 25 °C and 1.1 bar of ethylene. Toluene was used as the solvent and saturated with ethylene prior to the catalyst's introduction. Ethylene consumption, temperature, and pressure were monitored in real time using data acquisition and control software, enabling the acquisition of kinetic profiles. The polymerizations were run until a certain amount of ethylene was consumed. Polymerization reactions were quenched by the addition of acidified methanol. The polymer was collected and washed twice with methanol before drying.

Two different polymerization methodologies were applied for the preparation of the nanocomposite samples.

Method A: UA was reacted with TIBA (1:1 molar equivalent) for 15 min). Cp_2ZrCl_2 was precontacted with MAO solution in toluene for 15 min to obtain an Al/Zr ratio of about 1000. The mesoporous silica suspension (containing 100 mg of neat NMCM-41) and the UA comonomer precontacted with TIBA were successively introduced in the reactor. Next, the preactivated catalyst (in the homogeneous phase) was injected into the reactor, and the ethylene/UA copolymerization started.

Method B: In the reactor inerted with ethylene-saturated toluene, the required amount of MAO is injected in order to obtain an Al/Zr ratio of about 1000. Ethylene polymerization is initiated with the introduction of the zirconocene catalyst supported on the modified NMCM-41.

The polymerization conditions used and the corresponding catalytic activities are shown in Table 1. The different samples are named according to the methodology used for their preparation. Method A, in the absence of MCM-41 nanoparticles, was also used to prepare copolymers of ethylene with UA (REF 1 and REF 2 samples).

The UA content of representative samples was determined by ^1H -NMR spectroscopy using the method indicated in a previous work [10]. ^1H NMR spectra were obtained at 300 MHz using a Bruker MSL 300P spectrometer. 1,1,2,2-tetrachloroethane- d_2 was the used solvent. Polymer samples were observed at 380 K.

3.5. Characterization of the PE-UA-NMCM-41 Nanocomposites

3.5.1. Scanning Electronic Microscopy

Scanning electron micrographs were obtained on JEOL JSM-7001F equipment. SEM micrographs of the particles (SEI) were obtained using the secondary electron detector (SE, topography), and for the images of the nanocomposites (COMPO), the backscattered detector (BSE, composition contrast) was used.

3.5.2. Transmission Electronic Microscopy

Transmission electron micrographs were obtained with Hitachi 8100 equipment. Nanocomposites were deposited in a Cu/polymer grid holder.

3.5.3. Preparation of Films

The modified MCM-41/HDPE nanocomposites were processed as films (thickness ca. 250–300 μm) by compression molding in a Collin press between hot plates at 170 $^\circ\text{C}$ using a pressure of 2 MPa for 4 min, and then quenched down to room temperature with circulating water.

3.5.4. X-ray Diffraction Experiments

Wide-angle X-ray diffraction (WAXS) patterns were recorded in the reflection mode by using a Bruker D8 Advance diffractometer provided with a PSD Vantec detector (from Bruker, Madison, WI, USA). Cu $\text{K}\alpha$ radiation ($\lambda = 0.1542 \text{ nm}$) was used, operating at 40 kV and 40 mA. The parallel beam optics were adjusted by a parabolic Göbel mirror with a horizontal grazing incidence Soller slit of 0.12° and a LiF monochromator. The equipment was calibrated with different standards. A step scanning mode was employed for the detector. The diffraction scans were collected within the range of $2\theta = 1\text{--}43^\circ$, with a 2θ step of 0.024° and 0.2 s per step.

The estimation of hybrid crystallinity (f_c) was carried out at room temperature from WAXD profile deconvolution into the crystalline diffractions and the amorphous component using a fitting program. The error in the crystallinity determinations is estimated to be ± 4 units.

3.5.5. Thermogravimetric Experiments

The degradation processes were estimated by thermogravimetry using TA Instruments TGA Q500 equipment working under inert and oxidant atmospheres. The equipment was calibrated according to standard protocols. The sample weights ranged from 4 to 6 mg, and the heating rate was 10 °C/min.

3.5.6. Differential Scanning Calorimetry Measurements

Calorimetric analyses were carried out on a TA Instruments Q100 calorimeter connected to a cooling system and calibrated with different standards. The sample weights ranged from 5 to 7.5 mg. A temperature interval from −40 °C to 160 °C has been studied, and the heating rate used was 10 °C/min. For crystallinity determinations, a value of 290 J/g has been taken as the enthalpy of fusion of a perfectly crystalline material [59,60].

3.5.7. Viscoelastic Relaxation Study

Viscoelastic properties were measured in a Polymer Laboratories MK II dynamic mechanical thermal analyzer working in a tensile mode. The complex modulus and the loss tangent for each sample were determined at 1, 3, 10, and 30 Hz over a temperature range from −150 to 130 °C at a heating rate of 1.5 °C/min.

4. Conclusions

MCM-41 nanoparticles have been successfully attained for their use as a minor component in nanocomposites based on polyethylene and neat or modified NMCM-41 prepared by in situ polymerization. These materials have been synthesized by two different protocols, using UA to improve the interfacial adhesion between the hydrophobic matrix and the hydrophilic nanoparticles of silica: in the first one, the UA is incorporated into the polymeric chains and the NMCM-41 is neatly added into the reactor; and, in the second method, ethylene is polymerized, having previously functionalized the NMCM-41 with UA and supporting the catalyst onto these decorated nanoparticles. Concerning the catalytic characteristics, the presence of a small amount of UA, either in the neat copolymer or in the nanocomposite prepared under homogenous conditions (samples REF1 and A1), maintains high polymerization activity. Nevertheless, a higher amount of UA (~8 times) in the medium of reaction leads to a strong decrease of the polymerization activity, both for the copolymerization reactions performed in the absence or presence of neat NMCM-41 (samples REF2, A2, and A3). In spite of the high steric effect of the bulky protection agent used in this work (TIBA), protection of the polar carboxylic groups is not complete, contributing to the deactivation of the electrophilic catalyst active center ($\text{Cp}_2\text{Zr}^+\text{CH}_3$). An important reduction of activity is also noted in the systems prepared under supported conditions despite the lower UA concentration (samples B1 and B2). The steric hindrance of the support, some inefficient active site generation, and the proximity of UA polar groups to the catalyst active sites may explain this behavior. The thermal stability of nanocomposites is rather unaffected by the incorporation of either UA or NMCM-41 nanoparticles. A study of their phase transitions indicates that crystallites in the materials containing NMCM-41 are slightly thicker than those grown in the neat REF1 copolymer. Nevertheless, the degree of crystallinity is dependent on the synthetic protocol. On the other hand, NMCM-41 nanoparticles play a slight nucleating role in those nanocomposites where a low amount of UA was used during polymerization, independently of the synthetic approach employed. The presence of higher UA contents leads to a delay in the crystallization process. Regarding the morphological features of these nanocomposites, a less random distribution of NMCM-41 and the formation of agglomerates of larger size are observed in those materials prepared when nanoparticles were used neatly and under homogenous polymerization conditions. Furthermore, a higher content of UA during polymerization in this set of materials also worsens the dispersion of the silica nanoparticles. These morphological aspects affect the stiffness shown by the nanocomposites. Despite the fact that all of them show higher modulus values at 20 °C than those observed in the copolymer, the reinforcement

effect of NMCM-41 is larger in the materials where nanoparticles were decorated with UA in a previous stage and used further as catalyst support. Their slightly lower degree of crystallinity is compensated by the better adhesion between the two components at the interfaces promoted by the UA units existing on the surfaces of NMCM-41. Summarizing, incorporation of UA and a constant amount of NMCM-41 allows obtaining nanocomposites based on ethylene with a better mechanical performance in terms of rigidity (up to a 35% increase in the storage modulus), where the synthetic approach is important for the activity, the crystalline details, the morphological characteristics, and, accordingly, the final properties.

Supplementary Materials: The following supporting information can be downloaded at: <https://www.mdpi.com/article/10.3390/catal13081182/s1>. Figure S1: Nitrogen isotherms of MCM-41 and NMCM-41 (micro and nanoparticles, respectively); Figure S2: X-ray diffraction patterns at low angles for MCM-41 (black line) and NMCM-41 (blue line). Figure S3: FTIR spectra for pristine (blue line) and modified (red line) NMCM-41; Figure S4. Derivatives of thermogravimetry (DTG) curves attained from experiments performed under (a) inert and (b) air atmospheres for the samples REF1 and the different nanocomposites synthesized by the two in-situ polymerization protocols.

Author Contributions: Conceptualization, J.P.L. and M.R.R.; methodology, M.L.C., E.P., J.P.L. and M.R.R.; software, A.B. and E.P.; validation, M.L.C., A.B., E.P., J.P.L. and M.R.R.; formal analysis, M.L.C. and A.B.; investigation, M.L.C., A.B., E.P., J.P.L. and M.R.R.; resources, M.L.C. and M.R.R.; writing—original draft preparation, M.L.C. and M.R.R.; writing—review and editing, M.L.C., A.B., E.P., J.P.L. and M.R.R.; supervision, M.L.C., J.P.L. and M.R.R.; project administration, M.L.C. and M.R.R.; funding acquisition, M.L.C. and M.R.R. All authors have read and agreed to the published version of the manuscript.

Funding: This research was funded by MCIN/AEI/10.13039/501100011033, grant number MCIN/AEI/10.13039/501100011033. Funding from Fundação para a Ciência e Tecnologia (Project UIDB/00100/2020, Project UIDP/00100/2020, and Project LA/P/0056/2020) is also gratefully acknowledged.

Data Availability Statement: Data is contained within the article.

Acknowledgments: The authors are grateful to the Characterization Service for SEM, TGA, and X-ray Diffraction facilities and to the Service of Physicochemical Characterization of Polymers for DSC experiments, both services at ICTP-CSIC. The authors are also grateful to the personnel of these two Services for their support.

Conflicts of Interest: The authors declare no conflict of interest. The funders had no role in the design of the study, in the collection, analysis, or interpretation of data, in the writing of the manuscript, or in the decision to publish the results.

References

1. Mu, H.; Jian, Z. Stereoselective Copolymerization of Olefin with Polar Monomers to Access Stereoregular Functionalized Polyolefins. *Org. Mater.* **2022**, *4*, 178–189. [\[CrossRef\]](#)
2. Januszewski, R.; Dutkiewicz, M.; Kownacki, I. An Efficient Methodology for the Synthesis of Unique Functional Polyolefins. *Mater. Des.* **2021**, *206*, 109801. [\[CrossRef\]](#)
3. Dong, J.Y.; Hu, Y. Design and Synthesis of Structurally Well-Defined Functional Polyolefins via Transition Metal-Mediated Olefin Polymerization Chemistry. *Coord. Chem. Rev.* **2006**, *250*, 47–65. [\[CrossRef\]](#)
4. Boffa, L.S.; Novak, B.M. Copolymerization of Polar Monomers with Olefins Using Transition-Metal Complexes. *Chem. Rev.* **2000**, *100*, 1479–1493. [\[CrossRef\]](#)
5. Franssen, N.M.G.; Reek, J.N.H.; de Bruin, B. Synthesis of Functional ‘Polyolefins’: State of the Art and Remaining Challenges. *Chem. Soc. Rev.* **2013**, *42*, 5809–5832. [\[CrossRef\]](#) [\[PubMed\]](#)
6. Vicente, A.I.; Campos, J.; Bordado, J.M.; Rosário Ribeiro, M. Maleic Anhydride Modified Ethylene-Diene Copolymers: Synthesis and Properties. *React. Funct. Polym.* **2008**, *68*, 519–526. [\[CrossRef\]](#)
7. Mohanty, A.D.; Bae, C. Transition Metal-Catalyzed Functionalization of Polyolefins Containing CC, CC, and CH Bonds. *Adv. Organomet. Chem.* **2015**, *64*, 1–39. [\[CrossRef\]](#)
8. Goretzki, R.; Fink, G. Homogeneous and Heterogeneous Metallocene/MAO-Catalyzed Polymerization of Functionalized Olefins. *Macromol. Chem. Phys.* **1999**, *200*, 881–886. [\[CrossRef\]](#)
9. Ahjopalo, L.; Löfgren, B.; Hakala, K.; Pietilä, L.O. Molecular Modeling of Metallocene Catalyzed Copolymerization of Ethylene with Functional Comonomers. *Eur. Polym. J.* **1999**, *35*, 1519–1528. [\[CrossRef\]](#)

10. Santos, J.M.; Ribeiro, M.R.; Portela, M.F.; Pereira, S.G.; Nunes, T.G.; Deffieux, A. Metallocene-Catalysed Copolymerisation of Ethylene with 10-Undecenoic Acid: The Effect of Experimental Conditions. *Macromol. Chem. Phys.* **2001**, *202*, 2195–2201. [\[CrossRef\]](#)
11. Cerrada, M.L.; Benavente, R.; Pérez, E.; Moniz-Santos, J.; Campos, J.M.; Ribeiro, M.R. Ethylene/10-Undecenoic Acid Copolymers Prepared with Different Metallocene Catalysts. *Macromol. Chem. Phys.* **2007**, *208*, 841–850. [\[CrossRef\]](#)
12. Kaminsky, W. Polyolefin-Nanocomposites with Special Properties by in-Situ Polymerization. *Front. Chem. Sci. Eng.* **2018**, *12*, 555–563. [\[CrossRef\]](#)
13. Feldman, D. Polyolefin, Olefin Copolymers and Polyolefin Polyblend Nanocomposites. *J. Macromol. Sci. Part A* **2016**, *53*, 651–658. [\[CrossRef\]](#)
14. Campos, J.M.; Lourenço, J.P.; Cramail, H.; Ribeiro, M.R. Nanostructured Silica Materials in Olefin Polymerisation: From Catalytic Behaviour to Polymer Characteristics. *Prog. Polym. Sci.* **2012**, *37*, 1764–1804. [\[CrossRef\]](#)
15. Zou, H.; Wu, S.; Shen, J. Polymer/Silica Nanocomposites: Preparation, Characterization, Properties, and Applications. *Chem. Rev.* **2008**, *108*, 3893–3957. [\[CrossRef\]](#)
16. Chung, T.-S.; Jiang, L.Y.; Li, Y.; Kulprathipanja, S. Mixed Matrix Membranes (MMMs) Comprising Organic Polymers with Dispersed Inorganic Fillers for Gas Separation. *Prog. Polym. Sci.* **2007**, *32*, 483–507. [\[CrossRef\]](#)
17. Cecílio, D.M.; Cerrada, M.L.; Pérez, E.; Fernandes, A.; Lourenço, J.P.; McKenna, T.F.L.; Ribeiro, M.R. A Novel Approach for Preparation of Nanocomposites with an Excellent Rigidity/Deformability Balance Based on Reinforced HDPE with Halloysite. *Eur. Polym. J.* **2023**, *184*, 111765. [\[CrossRef\]](#)
18. Cecílio, D.M.; Fernandes, A.; Lourenço, J.P.; McKenna, T.F.L.; Ribeiro, M.R. Innovative Route for the Preparation of High-Performance Polyolefin Materials Based on Unique Dendrimeric Silica Particles. *Polym. Chem.* **2021**, *12*, 4546–4556. [\[CrossRef\]](#)
19. Bento, A.; Lourenço, J.P.; Fernandes, A.; Cerrada, M.L.; RosárioRibeiro, M. Functionalization of Mesoporous MCM-41 (Nano)Particles: Preparation Methodologies, Role on Catalytic Features, and Dispersion within Polyethylene Nanocomposites. *ChemCatChem* **2013**, *5*, 966–976. [\[CrossRef\]](#)
20. Bento, A.; Lourenço, J.P.; Fernandes, A.; Ribeiro, M.R.; Arranz-Andrés, J.; Lorenzo, V.; Cerrada, M.L. Gas Permeability Properties of Decorated MCM-41/Polyethylene Hybrids Prepared by in-Situ Polymerization. *J. Memb. Sci.* **2012**, *415*, 702–711. [\[CrossRef\]](#)
21. Campos, M.J.; Paulo Lourenço, J.; Pérez, E.; Cerrada, M.L.; Ribeiro, M.R. Self-Reinforced Hybrid Polyethylene/Mcm-41 Nanocomposites: In-Situ Polymerisation and Effect of MCM-41 Content on Rigidity. *J. Nanosci. Nanotechnol.* **2009**, *9*, 3966–3974. [\[CrossRef\]](#) [\[PubMed\]](#)
22. Campos, J.M.; Ribeiro, M.R.; Lourenço, J.P.; Fernandes, A. Ethylene Polymerisation with Zirconocene Supported in Al-Modified MCM-41: Catalytic Behaviour and Polymer Properties. *J. Mol. Catal. A Chem.* **2007**, *277*, 93–101. [\[CrossRef\]](#)
23. Ray, S.; Galgali, G.; Lele, A.; Sivaram, S. In Situ Polymerization of Ethylene with Bis(Imino)Pyridine Iron(II) Catalysts Supported on Clay: The Synthesis and Characterization of Polyethylene–Clay Nanocomposites. *J. Polym. Sci. A Polym. Chem.* **2005**, *43*, 304–318. [\[CrossRef\]](#)
24. Nakajima, H.; Yamada, K.; Iseki, Y.; Hosoda, S.; Hanai, A.; Oumi, Y.; Teranishi, T.; Sano, T. Preparation and Characterization of Polypropylene/Mesoporous Silica Nanocomposites with Confined Polypropylene. *J. Polym. Sci. B Polym. Phys.* **2003**, *41*, 3324–3332. [\[CrossRef\]](#)
25. Fu, S.; Sun, Z.; Huang, P.; Li, Y.; Hu, N. Some Basic Aspects of Polymer Nanocomposites: A Critical Review. *Nano Mater. Sci.* **2019**, *1*, 2–30. [\[CrossRef\]](#)
26. Tripathi, S.N.; Rao, G.S.S.; Mathur, A.B.; Jasra, R. Polyolefin/Graphene Nanocomposites: A Review. *RSC Adv.* **2017**, *7*, 23615–23632. [\[CrossRef\]](#)
27. Kageyama, K.; Tamazawa, J.I.; Aida, T. Extrusion Polymerization: Catalyzed Synthesis of Crystalline Linear Polyethylene Nanofibers Within a Mesoporous Silica. *Science* **1999**, *285*, 2113–2115. [\[CrossRef\]](#)
28. Ye, Z.; Zhu, S.; Wang, W.J.; Alsayouri, H.; Lin, Y.S. Morphological and Mechanical Properties of Nascent Polyethylene Fibers Produced via Ethylene Extrusion Polymerization with a Metallocene Catalyst Supported on MCM-41 Particles. *J. Polym. Sci. B Polym. Phys.* **2003**, *41*, 2433–2443. [\[CrossRef\]](#)
29. Cerrada, M.L.; Pérez, E.; Lourenço, J.P.; Campos, J.M.; Rosário Ribeiro, M. Hybrid HDPE/MCM-41 Nanocomposites: Crystalline Structure and Viscoelastic Behaviour. *Microporous Mesoporous Mater.* **2010**, *130*, 215–223. [\[CrossRef\]](#)
30. Barus, S.; Zanetti, M.; Lazzari, M.; Costa, L. Preparation of Polymeric Hybrid Nanocomposites Based on PE and Nanosilica. *Polymer* **2009**, *50*, 2595–2600. [\[CrossRef\]](#)
31. Cerrada, M.L.; Bento, A.; Pérez, E.; Lorenzo, V.; Lourenço, J.P.; Ribeiro, M.R. Hybrid Materials Based on Polyethylene and MCM-41 Microparticles Functionalized with Silanes: Catalytic Aspects of in Situ Polymerization, Crystalline Features and Mechanical Properties. *Microporous Mesoporous Mater.* **2016**, *232*, 86–96. [\[CrossRef\]](#)
32. Cerrada, M.L.; Pérez, E.; Lourenço, J.P.; Bento, A.; Ribeiro, M.R. Decorated MCM-41/Polyethylene Hybrids: Crystalline Details and Viscoelastic Behavior. *Polymer* **2013**, *54*, 2611–2620. [\[CrossRef\]](#)
33. Morrow, B.A. Chapter 3 Surface Groups on Oxides. *Stud. Surf. Sci. Catal.* **1990**, *57*, A161–A224. [\[CrossRef\]](#)
34. Jentys, A.; Pham, N.H.; Vinek, H. Nature of Hydroxy Groups in MCM-41. *J. Chem. Soc. Faraday Trans.* **1996**, *92*, 3287–3291. [\[CrossRef\]](#)
35. Landry, C.C.; Pappé, N.; Mason, M.R.; Apblett, A.W.; Tyler, A.N.; MacInnes, A.N.; Barron, A.R. From Minerals to Materials: Synthesis of Alumoxanes from the Reaction of Boehmite with Carboxylic Acids. *J. Mater Chem.* **1995**, *5*, 331–341. [\[CrossRef\]](#)

36. Gurian, P.L.; Cheatham, L.K.; Ziller, J.W.; Barron, A.R. Aluminium Complexes of N,N'-Ethylenebis(Salicylideneimine)(H₂ Salen). X-Ray Crystal Structures of [(Al(Salen))₂(μ-O)]·MeCN and [Al(OC₆H₂Me₃-2,4,6)(Salen)]. *J. Chem. Soc. Dalton. Trans.* **1991**, *6*, 1449–1456. [[CrossRef](#)]
37. Editors, G.; Milani, B.; Claver, C.; Kaminsky, W.; Funck, A.; Hähnsen, H.; Busico, V.; Trans, D.; Ciancaleoni, G.; Fraldi, N.; et al. An Investigation of the Influence of R on the Abilities of the Polar Monomers CH₂CH(CH₂)₈OR (R = Me, PhCH₂, Ph₃C, Me₃Si, Ph₃Si) to Participate in O- Rather than H₂-Coordination to Metallocene Alkene Polymerization Catalysts; an Unanticipated Role for Ether Oxygen Coordination in Promoting Polymerization. *Dalton. Trans.* **2009**, *41*, 8864–8877. [[CrossRef](#)]
38. Goretzki, R.; Fink, R. Homogeneous and heterogeneous metallocene/MAO-catalyzed polymerization of trialkylsilyl-protected alcohols. *Macromol. Rapid Commun.* **1998**, *19*, 511–515. [[CrossRef](#)]
39. Aaltonen, P.; Fink, G.; Löfgren, B.; Seppälä, J. Synthesis of Hydroxyl Group Containing Polyolefins with Metallocene/Methylaluminoxane Catalysts. *Macromolecules* **1996**, *29*, 5255–5260. [[CrossRef](#)]
40. Turunen, J.; Pakkanen, T.T.; Lijfgren, B. NMR Studies on the Reactivity of Aluminium Compounds with an Unsaturated Alcohol. *J. Mol. Catal. A Chem.* **1997**, *123*, 35–42. [[CrossRef](#)]
41. Silveira, F.; Alves, M.D.C.M.; Stedile, F.C.; Pergher, S.B.; dos Santos, J.H.Z. Microporous and Mesoporous Supports and Their Effect on the Performance of Supported Metallocene Catalysts. *J. Mol. Catal. A Chem.* **2010**, *315*, 213–220. [[CrossRef](#)]
42. Dong, X.; Wang, L.; Jiang, G.; Zhao, Z.; Sun, T.; Yu, H.; Wang, W. MCM-41 and SBA-15 Supported Cp₂ZrCl₂ Catalysts for the Preparation of Nano-Polyethylene Fibres via in Situ Ethylene Extrusion Polymerization. *J. Mol. Catal. A Chem.* **2005**, *240*, 239–244. [[CrossRef](#)]
43. Fischer, D.; Mülhaupt, R. Reversible and Irreversible Deactivation of Propene Polymerization Using Homogeneous Cp₂ZrCl₂/Methylaluminoxane Ziegler–Natta Catalysts. *J. Organomet. Chem.* **1991**, *417*, C7–C11. [[CrossRef](#)]
44. Marcilla, A.; Gómez-Siurana, A.; Berenguer, D. Study of the Influence of the Characteristics of Different Acid Solids in the Catalytic Pyrolysis of Different Polymers. *Appl. Catal. A Gen.* **2006**, *301*, 222–231. [[CrossRef](#)]
45. Sinfrônio, F.S.M.; Souza, A.G.; Santos, I.M.G.; Fernandes, V.J.; Novák, C.; Éhen, Z. Influence of H-ZSM-5, Al-MCM-41 and Acid Hybrid ZSM-5/MCM-41 on Polyethylene Decomposition. *J. Therm. Anal. Calorim.* **2006**, *85*, 391–399. [[CrossRef](#)]
46. Shirayama, K.; Kita, S.-I.; Watabe, H. Effects of Branching on Some Properties of Ethylene/α-Olefin Copolymers. *Die. Makromol. Chem.* **1972**, *151*, 97–120. [[CrossRef](#)]
47. Bunn, C.W. The Crystal Structure of Ethylene. *Trans. Faraday Soc.* **1944**, *40*, 23–25. [[CrossRef](#)]
48. Beck, J.S.; Vartuli, J.C.; Roth, W.J.; Leonowicz, M.E.; Kresge, C.T.; Schmitt, K.D.; Chu, C.T.W.; Olson, D.H.; Sheppard, E.W.; McCullen, S.B.; et al. A New Family of Mesoporous Molecular Sieves Prepared with Liquid Crystal Templates. *J. Am. Chem. Soc.* **1992**, *114*, 10834–10843. [[CrossRef](#)]
49. Popli, R.; Mandelkern, L. The Transition in Ethylene Copolymers: The β-Transition. *Polym. Bull.* **1983**, *9*, 260–267. [[CrossRef](#)]
50. Popli, R.; Glotin, M.; Mandelkern, L.; Benson, R.S. Dynamic Mechanical Studies of α and β Relaxations of Polyethylenes. *J. Polym. Sci. Polym. Phys. Ed.* **1984**, *22*, 407–448. [[CrossRef](#)]
51. Cerrada, M.L.; Benavente, R.; Pérez, E. Influence of Thermal History on Morphology and Viscoelastic Behavior of Ethylene-1-Octene Copolymers Synthesized with Metallocene Catalysts. *J. Mater. Res.* **2001**, *16*, 1103–1111. [[CrossRef](#)]
52. Cerrada, M.L.; Benavente, R.; Peña, B.; Pérez, E. The Effect of Thermal Treatment on the Structure and Relaxation Processes of Olefinic Polymers Synthesized with Metallocene Catalysts. *Polymer* **2000**, *41*, 5957–5965. [[CrossRef](#)]
53. Schatzki, T.F. Statistical Computation of Distribution Functions of Dimensions of Macromolecules. *J. Polym. Sci.* **1962**, *57*, 337–356. [[CrossRef](#)]
54. Boyd, R.H. Relaxation Processes in Crystalline Polymers: Experimental Behaviour—A Review. *Polymer* **1985**, *26*, 323–347. [[CrossRef](#)]
55. Ward, I. *Mechanical Properties of Solid Polymers*, 2nd ed.; John Wiley and Sons: Chichester, UK, 1983.
56. McCrum, N.; Read, B.; Williams, G. *Anelastic and Dielectric Effects in Polymeric Solids*; Dover Publications: New York, NT, USA, 1991.
57. Qiao, Z.A.; Zhang, L.; Guo, M.; Liu, Y.; Huo, Q. Synthesis of Mesoporous Silica Nanoparticles via Controlled Hydrolysis and Condensation of Silicon Alkoxide. *Chem. Mater.* **2009**, *21*, 3823–3829. [[CrossRef](#)]
58. Galarneau, A.; Villemot, F.; Rodriguez, J.; Fajula, F.; Coasne, B. Validity of the T-Plot Method to Assess Microporosity in Hierarchical Micro/Mesoporous Materials. *Langmuir* **2014**, *30*, 13266–13274. [[CrossRef](#)]
59. Quinn, F.A.; Mandelkern, L. Thermodynamics of Crystallization in High Polymers: Poly-(Ethylene). *J. Am. Chem. Soc.* **1958**, *80*, 3178–3182. [[CrossRef](#)]
60. Wunderlich, B. *Macromolecular Physics*; Academic Press: New York, NT, USA, 1980.

Disclaimer/Publisher's Note: The statements, opinions and data contained in all publications are solely those of the individual author(s) and contributor(s) and not of MDPI and/or the editor(s). MDPI and/or the editor(s) disclaim responsibility for any injury to people or property resulting from any ideas, methods, instructions or products referred to in the content.